Proceedings of the ASME 2010 3rd Joint US-European Fluids Engineering Summer Meeting and 8th International Conference on Nanochannels, Microchannels, and Minichannels
FEDSM-ICNMM2010
August 1-5, 2010, Montreal, Canada

FEDSM-ICNMM2010-30710

EWOD in coplanar electrode configurations

Rachid Malk
CEA, LETI, MINATEC,
F-38054 Grenoble, France

Arnaud Rival
CEA, LETI, MINATEC,
F-38054 Grenoble, France

Yves Fouillet
CEA, LETI, MINATEC,
F-38054 Grenoble, France

Laurent Davoust
CNRS – LEGI, Microfluidics, Interfaces & Particles Group,
BP 53, 38041 Grenoble Cedex9, France

ABSTRACT
This paper deals with ElectroWetting-On-Dielectric using AC voltage (AC EWOD) in both open and closed configuration. The open configuration is more convenient for fundamental studies and observations of electrowetting associated phenomena whereas the closed configuration is particularly adapted for practical use in a Digital lab-on-chips (DLC). Software developed for the study of electrowetting and droplet oscillations in coplanar electrode configuration are presented. Particular features of electrowetting are outlighted. Droplet oscillations and hydrodynamic induced flows in open coplanar configuration are considered and applications for DLC are illustrated in closed configuration.

INTRODUCTION
Digital lab-on-chips (DLC) are an alternative to conventional lab-on-chips based on continuous flow within microchannels. DLC consists in handling discrete amounts of liquid all over a surface. The droplets are considered as micro reactors inside which biological (or chemical) reactions can be individually achieved. Different physical mechanisms have thus been studied to develop processes at a scale of a droplet including thermocapillarity [1], surface acoustic waves (SAW), dielectrophoresis, asymmetric surface functionalisation [2],…

Among these mechanisms, electrowetting-on-dielectric is now a well-known technique in DLC. This phenomenon represents a very promising way of handling small volumes of liquid in micro-systems, with both a low power consumption and a high reliability. By electrically controlling the effective wettability of a droplet, liquid handling is made possible without the need for moving parts or external devices.
Basic operations such as drop displacement, drop mixing, drop coalescence or dispensing are fully achieved in DLC (Fig.1). As a consequence, EWOD actuation enables the integration of bio-protocols in a chip [3]. Immunoassay and PCR have been validated within an EWOD chip in [4], sample preparation for proteomics analysis with matrix-assisted laser desorption/ionisation mass spectrometer and DNA reparation are reported in [5] and [6] respectively.

Electrowetting on dielectric can be used in both open configuration and closed configuration. In the open configuration the observation of a sessile droplet profile is facilitated which makes this configuration more adapted for fundamental studies. Two major open configurations are classically considered: the ‘needle electrode configuration’ in which a wire counter electrode is immerged into the droplet and the ‘coplanar electrode configuration’. In the coplanar electrode configuration [7], the droplet spreads over two electrodes covered by insulating and hydrophobic layers. The equilibrium state is reached when the drop straddles both electrodes. A great advantage of coplanar electrodes is that the droplet flow (and oscillations) is (are) not disturbed by any needle counter-electrode. The open configuration used in this paper is the coplanar configuration (fig.1(a)).

The closed configuration (fig.1(b)) on the contrary, is more widespread for practical use within an integrated lab on chip owing to the ability to easily create, displace and split droplets. In this configuration, the droplet is placed between a grounded top cover plate and the chip substrate and droplet position is determined by the activated electrode. This closed configuration will be considered at the end of this article.

This paper is about electrowetting on dielectric using AC voltages. Two intriguing phenomena appearing on a droplet actuated with AC voltage are considered: droplet oscillations and hydrodynamic flows. Droplet oscillations induced by AC EWOD have been observed by different groups [8-10] on several electrowetting configurations. Induced flows are

reported by Kang [11] and steady streaming is likely to be the linking phenomena between oscillations and flows.

Here, we first describe EWOD chip technology and software used for Electrowetting on dielectric and droplet oscillations.The time average evolution of contact angle is then characterized using a brief parametric study supported by numerical simulation. This step also enables the validation of the pilling up technology of the chips. Then, the instantaneous effect of AC electrowetting on dielectric is illustrated through droplet oscillations. As a consequence of these oscillations, flows are generated and practical applications for digital lab-on-chip are discussed. We lastly demonstrate one of these applications in the closed configuration.

MATERIAL AND METHODS

Microfabrication

We describe in this section the process used for the fabrication of the two EWOD chips used for experiments in this paper: the 'open chip' for experiments in coplanar electrode configuration and the 'closed chip' for experiments with a cover plate. Most process is common to the two chips but the closed chip requires some additional steps.

The EWOD chips are microfabricated from a 200 mm silicon wafer. The fabrication process is based on conventional techniques of microelectronics and is entirely realized in the CEA-LETI-MINATEC clean rooms.

'Common process': The first step is a 1 µm thick silicon oxide layer obtained by a wet thermal oxidation (a). Then a first 200 nm thick AlCu metal layer is deposited (b). This step is followed by a photolithography and a dry etching step to pattern the electrical connection lines (20 µm width). A 300 nm thick dielectric layer of Si_3N_4 is then deposited using Plasma Enhanced Chemical Vapour Deposition (PECVD) (c). Tiny holes (15 µm x 15 µm) are photolithographied and etched in order to enable the connection between the first and the second metal layers obtained by the same process (200 nm thick AlSi) (d). This second metal layer is devoted to the electrode patterns. The use of two metal layers gives more flexibility in the design of the chips. Electrical line connection crossings are avoided and complex electrode areas can be patterned. Another PECVD step enables the covering of these electrodes with a 600 nm thick dielectric layer of Si_3N_4 (e). The electrical permittivity ε and breakdown strength of this layer are respectively 6.3 and 1 kV μm^{-1}. This insulating layer is opened by a photolithography and a dry etching to enable the electrical connection of the chip to the voltage generator.

'Open chip': The 22 x 22 mm chips are then individualized and covered with a 1 µm thick SiOC hydrophobic layer ($\varepsilon = 2.75\varepsilon_0$) which is a standard material used in CMOS technology. This SiOC (organosiloxane molecule) layer is deposited using PECVD (f). Contrary to Teflon®, SiOC is compatible with the process used in clean rooms. A large range of thickness is allowed from a few nm to several µm with good homogeneity and robustness [12]. As a surface layer, it must be chemically compatible with the use of biological samples and its properties must be reproducible in terms of contact angle and hysteresis. A low contact angle hysteresis and a high hydrophobic surface facilitate the displacement of the liquid droplet. Careful attention has thus been brought to the choice of the precursor and plasma conditions enabling interesting wetting properties: the zero contact angle between a water droplet and the air is 105° and 165° between a water droplet and silicone oil while the contact angle hysteresis is less than 10° in both cases.

'Closed chip': The active part is identical to open chips, but a 100µm thick dry film resist (Ordyl from Elga) is laminated on the Si_3N_4 layer and patterned by a contact photolithography step, creating the 100µm high wall defining different zones on the chip. A glass cover plate is placed on top of it confining the liquids on the chip. The plate is made from a 200mm glass wafer coated with ITO (Indium Thin Oxide) used as a transparent conductive layer. This wafer is sand-blasted (Anteryon B.V) to form through-holes of 1.6mm in order to create inlets for the different solutions. The hydrophobic SiOC layer is deposited on both chip and glass cover. The chip is filled with low density 5cPs silicon oil (RT5, Paragon Scientific) immiscible with water.

Closed chips have electrodes shapes different from the open configuration. They have for example a pattern of square electrodes on a line as presented in [13].

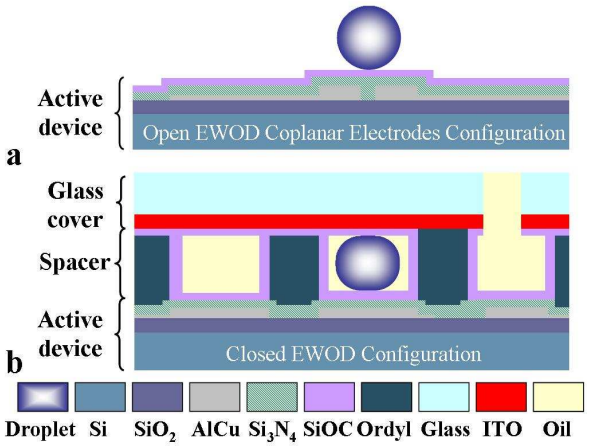

Fig.1 Diagram of the EWOD chip in open coplanar configuration (a) and closed configuration (b).

Experimental procedures

The experimental procedure used for experiments in coplanar electrode configuration is detailed here while the one used for experiment in closed configuration is described later for the sake of clarity.

An AC electrical signal was generated using a generator (Yokogawa) and a home-made amplifier. The maximum amplitude of the applied AC voltage, V, was 92 Vrms while the frequency, f, ranged from 150 Hz to 3 kHz. Out of this frequency range, the amplifier gain changes and the applied voltage shrinks. A CCD camera (Pixelfly) and a zoom lens were

used for image acquisition enabling the observation of droplet shape.
The experimental protocol of the EWOD experiment is similar to the one used in [14]. A picture of the droplet is taken at different values of the applied voltage. After each image acquisition, the voltage is set to zero and then incremented.
EWOD experiments in coplanar electrode configuration are performed with different parameters such as the electrical conductivity of the droplet and the electrode gap thickness. The lighting source is placed behind the droplet so as to create a backlight and minimize light reflection.
By using a stroboscopic lighting, droplet oscillations are made visible. The stroboscopic lighting is produced by a LED. EWOD actuation and stroboscopic lighting are controlled by the same function generator in order to ensure perfect synchronization. By shifting the phase between AC actuation and stroboscopic lighting, the instantaneous shape of the droplet can be observed.
As for flow observations, fluorescent beads are injected in the droplet to track the flow while fluoresceine is used to follow stirring. Excitation and emission wavelengths of both methods are 470 nm and 535 nm respectively.

Software package

Software package has been developed to enable the complete automation of data acquisition and data analysis for both EWOD and oscillation experiments. The experiment setup is driven by a Labview program. The program drives the CCD camera and the function generator and save images of the droplet corresponding to different wetting angle (in case of EWOD experiment) or different profile shape (in case of oscillation experiment). Once the experiments are achieved, they are analysed using a Graphical User Interface (GUI) developed on Matlab. Image analysis based on edge detection is performed and wetting angle is measured. For oscillation experiments, the GUI measures the wetting diameter, the droplet height and the wetting angle. Droplet profiles are decomposed into Legendre polynomials and eigenmodes oscillations can be precisely characterized. Numerical simulations using the extracted profile are then possible using Comsol Multiphysics with previous GUI. The droplet profiles are integrated into the geometric domain and electrostatic computation is carried out. A loop enables the implementation of the calculation using the next droplet profile. Accumulated surface charge and electric field repartition can thus be computed.

RESULTS AND DISCUSSION

Electrowetting in coplanar configuration, EWOD induced droplet oscillations and hydrodynamic flows are successively considered in this section. The first paragraph describes the electrowetting principles that are illustrated by a brief parametric study. The second paragraph focuses on the instantaneous effects of AC electrowetting and subsequent droplet oscillations and in the next paragraph, induced flows are finally considered.

EWOD in coplanar electrode configuration

The wetting angle of a droplet put over two coplanar electrodes recovered by insulated layers can be controlled by electrical voltage. This phenomenon illustrated on fig.2 is called Electrowetting on dielectric and has been introduced by Berge [15]. At zero voltage, a non wetting configuration is observed. On the contrary, when voltage is applied, electrical stresses appear which make the contact angle to decrease.

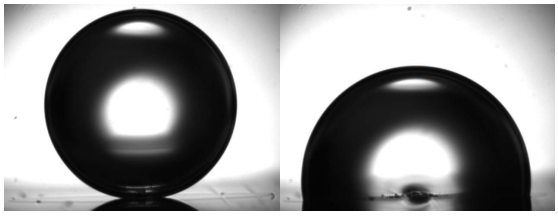

Fig.2 Contact angle change induced by EWOD in coplanar configuration. The voltage contact angles are (a) 165°at 0 Vrms and (b) 105° at 92 Vrms. Droplet volume is 1.5µl and ambient liquid is silicone oil..

The electrowetting phenomenon can be understood by using different physical approaches: the electromechanical approach, the Maxwell stress tensor approach, the thermodynamic approach and the energy minimization approach which are detailed in [16].
All these approaches can be related to Lippmann – Young equation governing the wetting of a droplet actuated with EWOD. Considering the droplet as a perfect conductor (hypothesis discussed in section 5.2) the Lippmann – Young equation in the 'classical' configuration reads:

$$\mathrm{Cos}\,(\theta_V) = \mathrm{Cos}\,(\theta_0) + (CV^2) / (2\gamma), \qquad (1)$$

where θ_0 is the zero voltage contact angle, θ_V is the contact angle modified by the electrical potential V, which in the case of AC voltage is the root mean square (RMS) voltage, C is the capacitance value per surface unit and γ is the surface tension between the droplet and the ambient phase. The second term of (eq.1) shows a competition between electric energy stored by surface unit ($1/2.CV^2$) which tends to make the droplet to wet and surface energy (γ) which is opposed to surface change. The contact angle modification of a droplet will thus depend on this ratio.
On the coplanar electrode configuration, the droplet straddles the two electrodes. Derived from the calculation presented in [17], and taking into account the serial insulating layers (dielectric layer: Si_3N_4, hydrophobic layer: SiOC), the equation (1) finally reads, by neglecting the influence of the thickness of the electrode gap:

$$\mathrm{Cos}(\theta_V) = \mathrm{Cos}(\theta_0) + \varepsilon_1 \varepsilon_2 V^2 / ((\varepsilon_1 d_2 + \varepsilon_2 d_1)\, 8\gamma)\,, \qquad (2)$$

where the subscripts 1 and 2 indicate the Si_3N_4 insulating layer and SiOC hydrophobic layer respectively, ε is the electrical permittivity and d is the layer thickness.

As the electrowetting stress depends on the square of the applied voltage, EWOD works whatever the sign of the applied voltage is and in particular when the voltage varies from positive to negative values as it occurs with AC voltage. In this case, the electrowetting stress displays a mean value and a time dependent part. The mean value of the stress monitors the mean contact angle of the droplet while the time dependent part induces oscillations. Using the root mean square value *Vrms*, eq (2) can be used to determine the mean contact angle evolution of the droplet.

Lippmann-Young equation predicts a parabolic relationship between contact angle and electrical voltage until reaching the total wetting of droplet. Yet, at high voltage, the contact angle saturates and the Lippmann-Young equation is no more valuable. The understanding of contact angle saturation is still a subject of debate and depending on experimental conditions; different mechanisms are likely to be involved [16].

Conductivity and frequency dependences:

Fig.3 shows the wetting of a 1.5µl PBS droplet surrounded by air versus the applied RMS voltage at 3 kHz. The electrode gap between the two electrodes is 3µm. The electrical conductivity of PBS was measured as σ =1.6 S/m while the theoretical electrical conductivity of ultra pure is σ =5.5e-6 S/m. In practise yet, the droplet is always more or less contaminated by impurities coming from its manipulation, contact with air and from the chip substrate which can modify the electrical conductivity. Surface tension is 73 mN/m in both cases. Good agreement between eq.2 and PBS curve is observed. This implies that the two hypotheses (perfect electrical conductor and no gap influence) are fully satisfied. It can be noticed that for such a coplanar configuration and such a voltage range, no configuration no contact angle saturation can be observed.

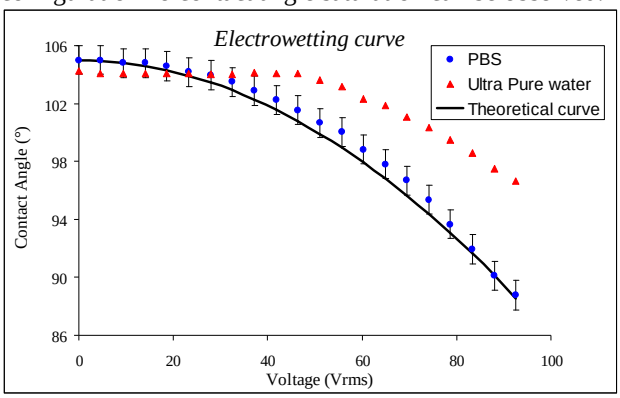

Fig.3 Electrowetting of PBS and ultra pure water droplets at 3 kHz. Error bars are estimated to be 2°.

When experiment is achieved with ultra pure water, a large deviation from theory is observed at 3 kHz. Moreover the wetting of the droplet displays a pure high frequency dependence between 300 Hz and 3 kHz which is not observed with PBS droplet (fig.4). The higher the frequency is, the higher the deviation is. At a frequency lower than 300 Hz, droplet profiles start to be blurred because of the large amplitude oscillations induced by the AC modulation which makes the contact angle measurement difficult to perform.

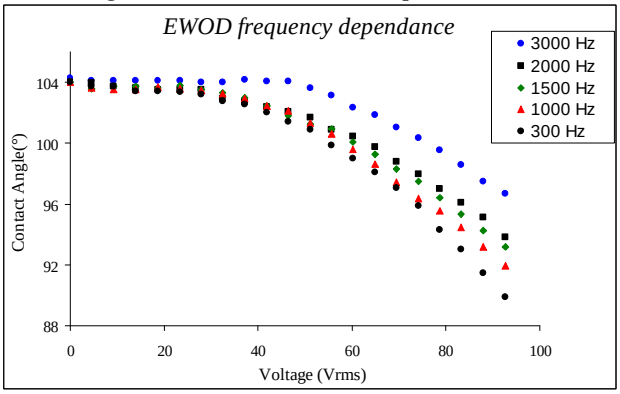

Fig.4 Electrowetting of an ultra pure water droplet at different frequencies.

The interpretation of the frequency and electrical conductivity dependence can be visualized by the numerical simulation. Droplet profiles are extracted from experiment and implemented into numerical simulation based on finite element method. In case of a PBS solution, the droplet is equipotential and its electrical potential is consistently found to be half the RMS applied voltage (fig.5 (a)). Charge carriers screen the electric field and the voltage drop is concentrated upon the dielectric layer.

For ultra pure water, on the contrary, the droplet is no more equipotential, voltage drop occurs both in the dielectric layer and in the droplet due to charge carriers that can no more follow the applied electric field (fig.5 (b)). As a consequence, the electrostatic energy stored in the underlying dielectric layer decreases and the electrowetting effect is consequently reduced.

Jones [7] introduced RC circuit model to estimate the critical frequency separating EWOD from liquid dielectrophoresis. Far below this critical frequency, the perfect conductor hypothesis is valid and electrowetting occurs while far above it, the liquid behaves as a dielectric medium. Critical frequency of PBS droplet is 66 MHz, while its value for ultra pure water is 250 Hz, which accounts for experimental observations achieved at neighbouring frequencies.

All other experiments have thus been performed with PBS solution.

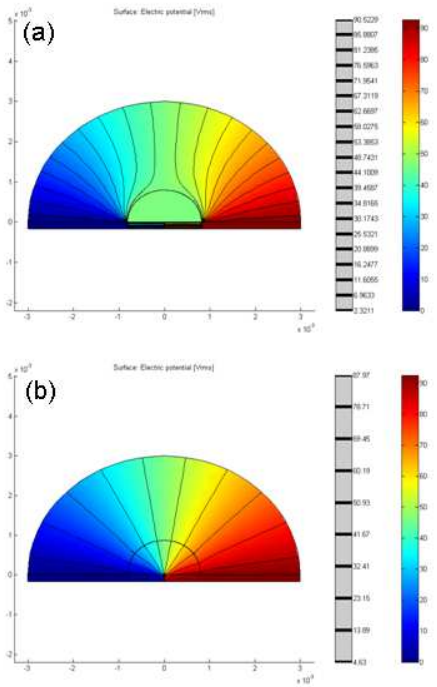

Fig.5 Electric potential distribution in and around a PBS droplet(a) and an ultra pure water droplet (b) as numerically calculated at 3kHz.

Electrode gap thickness influence:

The electrode gap is defined as the spacing between the two coplanar electrodes. Eq.2 was established by making the hypothesis of insignificant electrode gap and the good agreement with previous experiment using PBS droplet shows that this hypothesis is validated for a 3µm gap.

We now perform EWOD experiments with several electrode gaps ranging from 3 to 200µm. A 1.5µl PBS droplet is used and frequency is fixed at 3000 kHz.

Fig.6 shows that the larger the electrode gap is, the higher the contact angle is. At a high voltage, the separation between the different curves is found to be about 3° for 200 µm gap compared to a 3 µm gap.

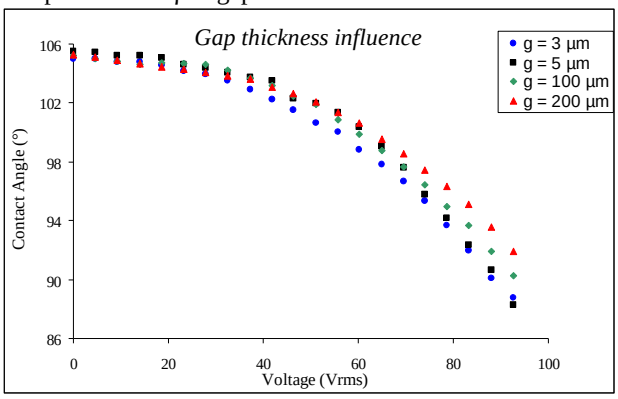

Fig.6 Impact of the Electrode gap widths upon electrowetting of a PBS droplet at 3 kHz.

As it can be expected, contact angles are higher with chips having large electrode gaps. This is due to the global electrical capacitance through the dielectric layers which is reduced and this can be easily checked numerically by calculating the surface charge accumulated at the droplet-solid interface. Surface charge is calculated from the Gauss' law which reads, at the liquid-solid interface:

$$qs = \left\| \varepsilon \boldsymbol{E}\cdot\mathbf{n} \right\| \quad , \qquad (3)$$

where $\left\| a\cdot\mathbf{n} \right\|$ denotes the jump of a quantity a across a dividing interface, $\boldsymbol{E}$ is the electric field vector and $\boldsymbol{n}$ is the outward unit normal vector. Here again, droplet profile used for computation is extracted from imaging of experiments.

As AC voltage is used, root mean square quantities have to be considered. Complex values are first implemented on Comsol and the calculation of root mean square quantities is achieved using the following relationship:

$$A_{rms} = \text{sqrt}(1/2*\text{real}(A*\text{conj}(A))) \, , \qquad (4)$$

where A is a complex quantity which can be a scalar (electrical potential for example) or a vector (electric field for example) and conj(A) is the complex conjugate.

Using eq(3) and eq(4), root mean square surface charge is calculated on the liquid-solid interface and is plotted on fig.7 :

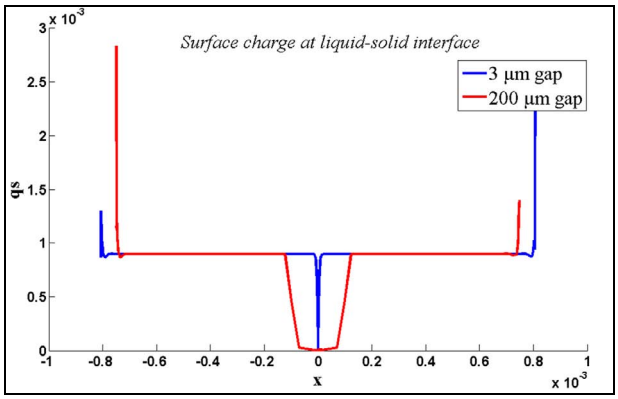

Fig.7 Surface charge along liquid-solid interface. Extension along x axis shows that the wetting diameter is higher for a 3µm gap, which is consistent with fig(6).

The surface charge distribution displays singularities at the triple points due to sharp edge effect. Exact estimation of peak values is a real issue [18] and is beyond the scope of this study. Thus, peak values are not relevant.

Far away from singularities, one can see that on the electrode gap, no surface charge is accumulated. The only non vanishing surface charge is located at the surfaces over the two electrodes. Consequently, the surface above the electrode gap does not store electrostatic energy and does not contribute to droplet electrowetting. As a result, 3 µm gap chips are thus more efficient from electrowetting point of view than 200 µm gap.

Contact angle evolution in coplanar electrode configuration follows thus a more adapted equation involving the electrode gap:

$$\mathrm{Cos}(\theta_V) = \mathrm{Cos}(\theta_0) + A_{rel}.\ \varepsilon_1\ \varepsilon_2 V^2 / ((\varepsilon_1 d_2 + \varepsilon_2 d_1)\ 8\gamma)\ , (5)$$

with $A_{rel} = (2R_{wet}\text{-}g)/(2R_{wet})$, the relative surface area where R_{wet} is the wetting radius and g is the electrode gap. With extracted experimental profiles, calculation of the relative surface A_{rel} is achieved; for a 3µm gap, its mean value is 0.99 while for a 200µm gap its decreases to 0.87. Theoretical contact angles deduced from eq.(5) and plotted on fig.8 show a difference of about 3° at 92 Vrms which compares favourably with our experimental observations. A similar expression about the influence of electrode gap can be found in [19].

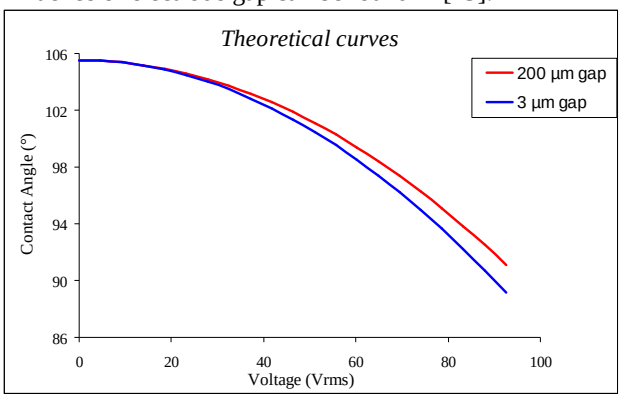

Fig.8 Theoretical electrowetting curves using eq.(5). A large electrode gap (200µm) decreases the electrical capacitance and therefore reduces the electrowetting efficiency.

Droplet oscillations

Previous section focused on the evolution of the mean contact angle, imaged under classical lighting source. Yet by shifting to the synchronized stroboscopic lighting droplet oscillations can be made evident. These oscillations result from the time-dependent component of the electrowetting stress and thus can not be visible with DC voltage.

Depending on the frequency of the applied voltage, different profile shape can be observed (fig. 9).

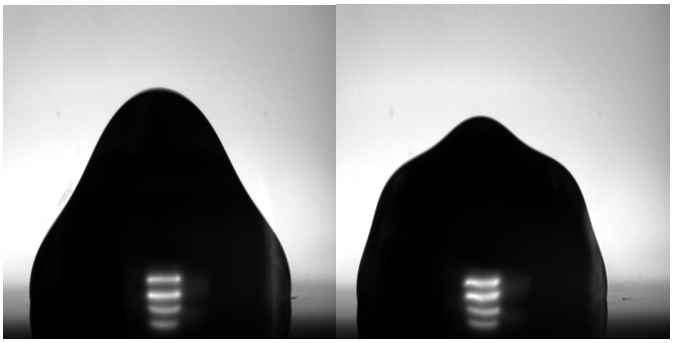

Fig.9 1.5 µl droplet shape at 200 Hz (a) and 600 Hz (b) made evident with stroboscopic lighting.

Droplet oscillations have been studied by Kelvin [20] and Rayleigh [21]. Later, resonance frequencies ($f_c = \omega_c / 2\pi$) of a spherical inviscid droplet have been calculated by Lamb [22]:

$$\omega_c^2 = n\ (n\text{-}1)\ (n\text{+}2)\ \gamma / \rho\ R^3, \qquad (6)$$

where n is the an integer value of 2 or higher representing the n^{th} mode of oscillations, R is the volume-averaged radius, and ρ is the density. Note that n=1 corresponds to pure translation.

Oscillation modes are recognizable by the number of lobes. Assuming axisymetrical oscillations, droplet profile can be expressed as a series of Legendre polynomials P_n :

$$r = R + \sum a_n P_n(\mathrm{Cos}\ (\theta)), \qquad (7)$$

where a_n is the amplitude of the n^{th} oscillation mode. Each Legendre polynomial represents a characteristic oscillation shape (fig.10) and the droplet profile is expressed as a linear combination of these shapes.

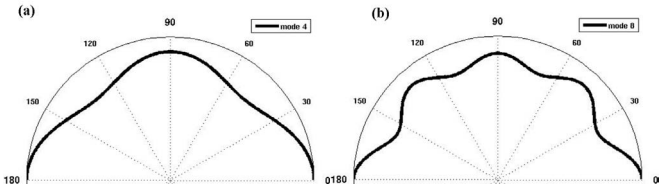

Fig.10 Characteristic droplet shape using Legendre polynomials of (a) degree 4 and (b) degree 8.

Decomposition into Legendre polynomials is achieved by the GUI using a least mean square algorithm. As oscillations are symmetrical, the amplitude of the odd modes is negligible with respect to the amplitude of even modes. Identification of oscillating modes up to the 12^{th} order is realized, beyond this eigenmode, amplitudes are so small that they are no more significant.

A 1.5µl PBS droplet is put on the 3µm gap chip. For each frequency ranging from 150 Hz to 1100 Hz an image of the oscillating drop is acquired and the frequency is incremented. In order to keep a constant volume during all the experiments, sacrificial droplets are placed around the studied droplet, and after each frequency implementation, the studied droplet is removed and replaced by another one. For reproducibility, silicone oil is deposited on the chip substrate thereby allowing slipping condition at the triple contact line.

Experiments show that droplet oscillates at a frequency which is exactly twice the input frequency. This is due to the electrowetting stress which is proportional to the square of the applied voltage [23] and input frequencies at which oscillation resonance is likely to occur are computed in tbl.1 from eq.(6).

	Mode 4	Mode 6	Mode 8	Mode 10	Mode 12
fc(Hz)	216	394	601	835	1092

Tbl. 1 Input resonant frequency of a 1.5µl droplet based on Lamb's theory.

The amplitude of each shape mode is strongly dependent on the input frequency as illustrated on fig.11. Frequency domains corresponding to each eigenmode can be observed: from 150 Hz to 250 Hz, the 4th eigenmode dominates, from 250 Hz to 450 Hz the 6th eigenmode dominates and so on. For each frequency domain, the dominant mode displays an amplitude peak corresponding to resonance. Oscillation amplitudes decreases as the actuation frequency increases and it can be checked from tbl.l that the peaks occur at frequencies which are closed to the Lamb's input resonant frequencies. As the frequency range starts at 150 Hz, the curve of the second mode (with theoretical input resonant frequency at 70 hz) is not represented for the sake of clarity, even though it has been taken into account in the decomposition polynomial process.

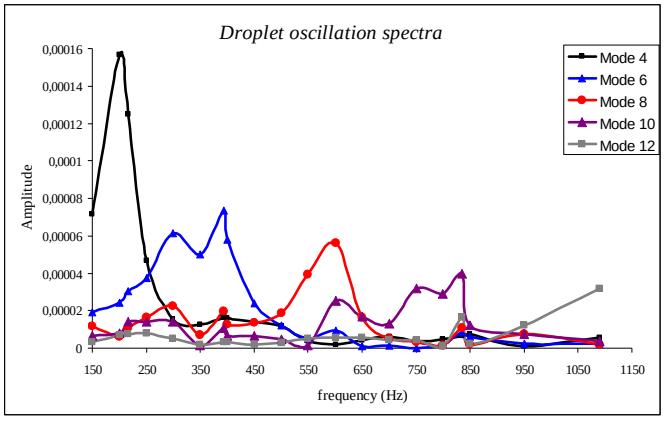

Fig.11 Oscillation spectra of a 1.5µl PBS droplet in air against the actuation frequency.

Interestingly, the curves display some subharmonic modes (200 Hz, 300 Hz…), second-order interactions between shape modes may be involved.
These oscillations have been observed with different ambient phase such as dodecane and silicone oil. While the droplet is oscillating, induced flows are created.

Induced hydrodynamic flows

Steady streaming flows:

When AC EWOD is actuated, flows are generated inside and outside the droplet through a mechanism called steady streaming. Steady streaming is a phenomenon associated with non linear effects that has been extensively studied [24, 25] and represents the nonzero mean flow induced by oscillatory motion. This phenomenon is observed in diverse areas including acoustic flows and sediment transport and good agreement between experimental observations of induced EWOD flows and numerical model based on oscillating droplet is reported by Ko [26].
Hydrodynamics flows induced by electrowetting can be made evident using fluorescent beads as tracers. Flow can be visualised from the waist of a laser sheet crossing vertically the droplet as reported in [11].
Surface observation is also possible which the type of visualization we use for our experiments in coplanar electrodes. We also use silicone oil as ambient phase to limit beads adsorption on the chip surface. In these experimental conditions, a steady flow is observed with typical mean velocity estimated to be around 1 mm/s. The increase of time acquisition allows to visualize flow streamlines and quadripolar structure flow is clearly made evident. By shifting to stroboscopic lighting, droplet shape and hydrodynamic can be observed simultaneously as shown on fig.12. Experiments achieved with other type of beads (hollow glass beads with density of 0.3) demonstrate a similar behaviour. Moreover, velocity field clearly displays frequency dependence with high velocity at low frequencies (150 hz) while the flow velocity is attenuated at high frequency (3000 Hz). A modal analysis with silicone oil as ambient phase similar to the one used in the previous paragraph as well as particle velocity measurement would be interesting but this goes beyond the scope of this paper.

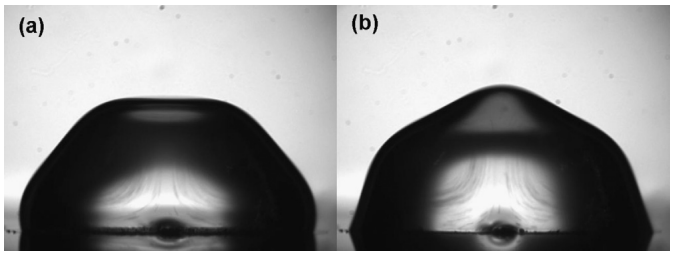

Fig.12 Side view of a droplet containing fluorescent beads visualized with stroboscopic lighting at 150 Hz. Phase lag is (a) 0° and (b) 90°. Input frequency is 150 Hz ([27]).

Applications in open configuration:

The tempting idea of exploiting these flows for practical use within a DLC represents a real issue. To complement the digital toolbox based on EWOD microfluidics, such a flow could be considered as a means of developing new basic operations. Two main applications can already be considered.

Cells or macromolecules handling:

In [26], AC EWOD is used to produce hydrodynamic jet around an oscillating bubble. Depending on the input frequency, different jet patterns and velocities are observed and potential applications aimed by authors are jet vectoring and particles handling.
On chip cell manipulation has been achieved by Chung at al. in [28]. Biological cells such as fish eggs and water fleas can be captured and released by an oscillating bubble. Once captured, the cells are transported by moving bubble using EWOD actuation. Eventhough oscillations of the bubbles are achieved by acoustic waves in [28], adaptation using AC EWOD as oscillation generator mechanism should produce the same results.

Cell manipulation could also be achieved within the droplet as suggested in [27]. Vortex flows are generated and polymer beads can be concentrated within vortex centers. By adjusting input frequency, droplet shape is modified and the position of the vortices on the droplet surface can be precisely controlled (fig.13), reproducibility and reversibilty of displacements have been observed. The ability to concentrate cells at a precise location along drop surface can be used as a means to facilitate interactions between a molecules and a target particules for instance.

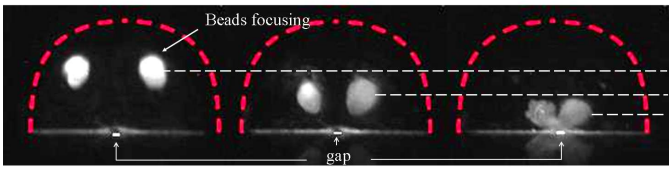

Fig.13 Change of positions of agglomerated beads realized by frequency shifting. Input frequencies for the three images are 150, 600 and 3000 Hz from left to right respectively. Mean droplet profile is represented by the red dashed- line.

Mixing enhancement:
In [8], mixing inside a droplet is achieved by induced flows using AC EWOD. A droplet containing food coloring was used to visualize the flows and mixing is realized within a motioless droplet.
In [9], mixing is also achieved within a droplet. The configuration here is slightly different whith a needle electrode and the oscillations are created by a repeted attaching-detaching of the droplet to the needle electrode.
Mixing at a scale of one millimetric droplet is a real issue of microfluidics and a key point for the development of digital microfluidics. We demonstrate in the following section that mixing can also be enhanced in a closed configuration.

Demonstration in closed configuration:
In this paragraph, the mixing process inside droplets in a closed EWOD configuration is considered. (fig.14). Droplets on the chip are generated as described in [13]. As presented before, the droplets are confined between the chip and a cover separated by a wall 100µm thick. The droplets are therefore squeezed and have a parallelipedic shape. This shape enables almost a planar configuration and provides a great reproducibility of the droplets volumes (less than 0.5% variation in droplet formation). Droplets visualization is made through a binocular stereomicroscope (Stereo Lumar, Zeiss).
We first analyze 10µm fluorescent beads inside droplet under 60V DC and 60V AC (70Hz) actuations (fig. 14 (a) and (b) respectively). One can see that the beads are completely immobile in DC actuation, whereas the 70Hz actuation shows strong beads recirculation: four vortices are created at the corners of the parallelipedic droplet. Top right and bottom left vortices turn clockwise, the two others vortices turn counterclockwise. Due to their frequency dependence, it seems obvious that the recirculation has the same origin as the one observed in open configuration, namely the oscillations at the triple lines.

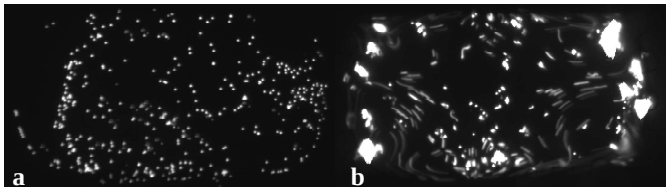

Fig.14 Images of a double droplet containing fluorescent 10µm beads (a) In DC actuation (b) in AC at 70Hz.

We further characterize the effect of these AC recirculations on mixing in static droplets. Fig.15 describes the experiments. A FP488 fluorescent droplet (Fluoprobes488, Interchim) and a non fluorescent one are brought together at the same speed from opposite direction until they coalesce. The double droplet remains at the same position by keeping the electrodes below it activated. Mixing between the two droplets immediately occurs after coalescence. Top view images of the droplet are taken as mixing progress and the standard deviation of the grey levels inside the droplets are plotted as a function of time as presented in [29].

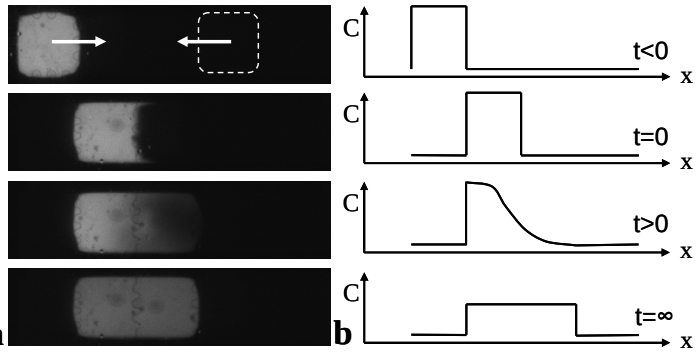

Fig.15 DC mixing experiment (a) Successive images of mixing droplets (b) The corresponding fluorescence intensity profiles.

In fig.16 the plots of the percentage of standard deviation (Std) of the fluorescence intensity inside the droplet for a 60V DC actuation and two 60V AC actuations frequencies are presented. Mixing is considered complete when the Std is less than 10% which corresponds to the measurement error. One can see that mixing time for DC actuation takes more than 1500 seconds. This mixing time originates from chemical diffusion kinetics of FP488 since no internal flow is observed. Mixing time is drastically reduced when the actuation is an AC voltage. Less than 1000 seconds at 3000Hz and less than 300 seconds at 70Hz are necessary to complete mixing within the resulting droplet.

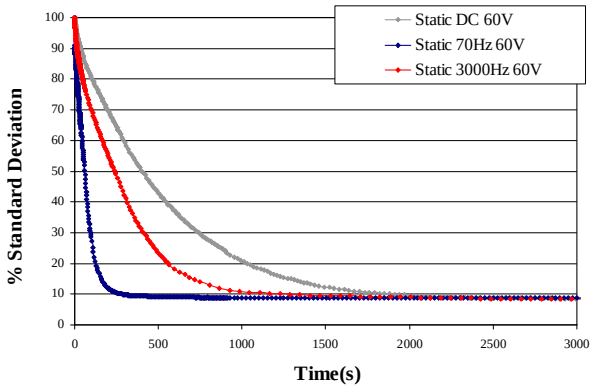

Fig.16 Percentage of standard deviation of the fluorescence intensity as a function of time during diffusion process of FP488 fluorescent molecules inside a static droplet at different actuation frequencies, 60V DC, 60V AC 70Hz and 60V AC 3000Hz.

These results show that even if it remains not much studied, AC actuation in closed EWOD microsystems has a great impact on flows inside the droplets. We believe that AC driven flows could reveal to be very important for theoretical studies as well as for practical applications such has mixing in DLC for instance.

CONCLUSION

A general study about AC EWOD is proposed all along this paper. Electrowetting in coplanar configuration, droplet oscillations and EWOD induced flows have been successively considered.

A parametric experimental study of EWOD supported by numerical model illustrates the influence of electrical conductivity, input frequency and gap thickness on the droplet wetting, and characterizes time-averaged effects of AC EWOD. As for time-dependent effects, they are analyzed through droplet oscillations. Oscillations spectra have been plotted using experimental droplet profiles and good agreement with Lamb's theory is observed. When injecting beads in such oscillating droplet, steady streaming is made evident. This paper shows that this phenomenon also occurs in closed configuration and can be used to efficiently enhance mixing.

ACKNOWLEDGMENTS

Put acknowledgments here.

REFERENCES

[1] Yarin, A.L.; Liu, W.; Reneker, D.H. Motion of droplets along thin fibers with temperature gradient, *J. Appl. Phys.* 91 (7) (2002) 4751, 4760.

[2] Buguin, A.; Talini, L.; Silberzan, P. Ratchet-like topological structures for the control of micro-drops, *Appl. Phys. A* 75 (2002) 207–212.

[3] Fouillet, Y.; Jary, D.; Chabrol, C.; Claustre, P.; Peponnet, C. Digital microfluidic design and optimization of classic and new fluidic functions for lab on chip systems, *Microfluid. Nanofluid., 2008,* (4), 159-165.

[4] Sista, R.; Hua, Z.; Thwar, P.; Sudarsan, A.; Srinivasan, V.; Eckhardt, A.; Pollack, M.; Pamula, V. Development of a digital microfluidic platform for point of care testing, *Lab Chip*, 2008, 8, 2091–2104.

[5] Wheeler, A.R.; Moon, H.; Bird, C.A.; Ogorzalek Loo, R.R.; Kim, C.J.; Loo, J.A.; Garrell, R.L. Digital Microfluidics with In-Line Sample Purification for Proteomics Analyses with MALDI-MS, *Anal. Chem.* 2005, 77, 534-540 .

[6] Jary, D.; Chollat-Namy, A.; Fouillet, Y.; Boutet, J.; Chabrol, C.; Castellan, G.; Gasparutto, D.; Pepponet, C. DNA repair enzyme analysis on EWOD fluidic microprocessor, *NSTI Nanotech*, 2006 Technical Proceedings, vol 2, pp :554–557

[7] Jones, T.B.; Gunji, M.; Washizu, M.; Feldman, M.J. Dielectrophoretic liquid actuation and nanodroplet formation, *Journal of applied Physics 2001*, Vol. 89, No. 3.

[8] Miraghaie, R.; Sterling, J. D.; Nadim, A. Shape oscillation and internal mixing in sessile liquid drops using electrowetting-on-dielectric (EWOD), *NSTI-Nanotech*, 2006, (*2*), 610-613.

[9] Mugele, F.; Baret, J.C.; Steinhauser, D. Microfluidic mixing through electrowetting-induced droplet oscillations, *Appl. Phys. Lett.*, 2006, 88.

[10] Sen, P.; Kim, C. J. Capillary Spreading Dynamics of Electrowetted Sessile Droplets in Air, *Langmuir*, 2009, 25 (8), 4302-4305

[11] Ko, S. H.; Lee, H.; Kang, K. H. Hydrodynamic flows in electrowetting, *Langmuir*, 2008, (*24*), 1094-1101.

[12] Thery, J.; Borella, M.; Le Vot, S.; Jary, D.; Rivera, F.; Castellan, G.; Brachet, A.G.; Plissonnier, M.; Fouillet, Y. Sioc as a hydrophobic layer for electrowetting on dielectric applications, *Proceedings of µTas 2007*, (1), 349-351, ISBN : 978-0-9798064-0-7.

[13] Fouillet, Y.; Jary, D.; Brachet, A.G. ; Berthier, J.; Blervaque, R. ; Davoust, L., Roux, J.M. ; Achard, J.L. ; Peponnet, C. Ewod Digital Microfluidics for Lab On A Chip, *Proceedings of ASME ICNMM2006.*

[14] Berry, S.; Kedzierski , J.; Abedian, B. Low voltage electrowetting using thin fluoroploymer films, *J. Colloid Interface Sci.* , 2006, 303, 517-524.

[15] Berge B 1993 Electrocapillarité et mouillage de films isolants par l'eau *C. R. Acad. Sci.* II 317 157.

[16] Mugele, F.; Baret, J.C. Electrowetting: from basics to applications, J. Phys.: Condens. Matter **17** (2005) R705–R774.

[17] Cooney, C.G.; Chen, C.Y.; Emerling, M.R.; Nadim, A.; Sterling, J. D. Electrowetting droplet microfluidics on a single planar surface, *Microfluid. Nanofluid.*, 2006, 2, 435–446.

[18] Vallet, M.; Vallade, M.; Berge, B. Limiting phenomena for the spreading of water on polymer films by electrowetting, 1999, *Eur. Phys. J.* B 11 583.

[19] Yi, U. C.; Kim, C. J Characterization of electrowetting actuation on addressable single-side coplanar electrodes, J. Micromech. Microeng. 16**,** 2006, 2053–2059.

[20] Lord Kelvin, Math. Phys. Pap. 3, 384, 1890.
[21] Lord Rayleigh, the Theory of Sound, 1894.
[22] Lamb, H. *Hydrodynamics*, Cambridge University Press, 1932.
[23] Oh, M.; Ko, S.H.; Kang, K.H. Shape Oscillation of a Drop in ac Electrowetting, *Langmuir* 24, 8379, 2008.
[24]Batchelor, G.K. An Introduction to Fluid Dynamics, Cambridge University Press, 1967.
[25] Riley, N. Steady streaming, *Annu. Rev. Fluid Mech.* 33:43-65, 2001.
[26] Ko, S. H.; Lee, S. J.; Kang, K. H. A synthetic jet produced in aqueous solution, *Applied Physics Letters*, 2009, 94, 194102.
[27] Malk, R.; Fouillet, Y.; Davoust, L. Rotating flow within a droplet actuated with AC EWOD, *Sens. Actuators B: Chem.* (2010), doi:10.1016/j.snb.2009.12.066.
[28] Chung, S. K.; Cho, S. K. On-chip manipulation of objects using mobile oscillating bubbles; J. Micromech. Microeng. ,18 (2008) 125024.
[29] Paik, P.; Pamula, V.K.; Fair, R.B. Rapid droplet mixers for digital microfluidic systems. *Lab Chip*, 2003, 3, 253–259.